Inorganic Chemistry
Article

Inorg. Chem. **2010**, *49*, 4843–4853 **4843**
DOI: 10.1021/ic902374t

Self-Association of Ruthenium(II) Polypyridyl Complexes and Their Interactions with Calf Thymus DNA

Satish S. Bhat,[†] Avinash S. Kumbhar,*[,†] Peter Lönnecke,[‡] and Evamarie Hey-Hawkins[‡]

[†]*Department of Chemistry, University of Pune, Pune-411007, India, and* [‡]*Faculty of Chemistry and Mineralogy, Department of Inorganic Chemistry, Johannisallee 29, Universität Leipzig, 04103 Leipzig, Germany*

Received December 1, 2009

Complexes of the type $[Ru(N-N)_2(bxbg)]Cl_2$ where N−N is 2,2′-bipyridine (bpy) (**1**), 1,10-phenanthroline (phen) (**2**), dipyrido [3,2-*d*:2′,3*f*] quinoxaline (dpq) (**3**), and dipyrido[3,2-*a*:2′,3′-*c*]phenazine (dppz) (**4**) which incorporate the bis(*o*-xylene)bipyridine glycoluril (bxbg) as the ancillary ligand have been synthesized and characterized by IR, NMR, UV−visible, luminescence, ESI-MS, cyclic voltammetry, and spectroelectrochemistry. The bis(*o*-xylene)bipyridine glycoluril initiates a head to head association which act as the nucleation point for the further growth in two direction by head-to-head and tail-to-tail self-association resulting in formation of aggregates in water which have been investigated by ^{1}H NMR, NOESY, steady state luminescence dilution experiments, and electron microscopy studies. The self-association has been confirmed by single crystal X-ray analysis of complex **2**. Electrochemical and spectroelectrochemical studies in acetonitrile show that these complexes undergo reversible one electron oxidation from Ru^{II} to Ru^{III}. The binding of these complexes with calf thymus DNA (CT-DNA) has been studied by absorption titration, steady-state and time-resolved emission measurement experiments, to investigate the influence of the ancillary ligand. The binding ability of these complexes to DNA is dependent on the planarity of the intercalative polypyridyl ligand which is further affected by the bis(*o*-xylene)bipyridine glycoluril ancillary ligand.

Introduction

Ruthenium(II) polypyridyl complexes have received much interest because of their extensive applications in the field of photochemistry, photophysics, and biochemistry. In particular, their important application as probes of DNA structure, DNA mediated electron transfer, and DNA foot printing agents are well-known.[1−7] The strong absorbance caused by metal to ligand charge transfer (MLCT), the luminescent characteristics, and their perturbations upon binding to DNA provide practicable means to explore their DNA binding mechanisms.[8−14] The versatility of these complexes is modulated by the ligand set, which controls whether the complex is an intercalator, hemi-intercalator, or electrostatic binder.[8−15] In general ruthenium polypyridyl intercalators like $[Ru(bpy)_2(dppz)]^{2+}$ and $[Ru(phen)_2(dppz)]^{2+}$ (Scheme 1) have binding affinities in the order of 10^6-10^7, while electrostatic binders like $[Ru(bpy)_3]^{2+}$ have binding affinities in the order of 10^3.

Mixed-ligand ruthenium(II) complexes can be modified in three dimensions to adapt to the DNA helix.[16−18] The ancillary ligand of polypyridyl ruthenium(II) complexes

*To whom correspondence should be addressed. E-mail: askum@chem.unipune.ernet.in. Fax: (+91)-020-25691728.

(1) Erkkila, K. E.; Odom, D. T.; Barton, J. K. *Chem. Rev.* **1999**, *99*, 2777–2795.
(2) Metcalfe, C.; Thomas, J. A. *Chem. Soc. Rev.* **2003**, *32*, 215–224.
(3) Sigman, D. S.; Mazumder, A.; Perrin, M. D. *Chem. Rev.* **1993**, *93*, 2295–2316.
(4) Dandlier, P. J.; Holmlin, R. E.; Barton, J. K. *Science* **1997**, *274*, 1465–1468.
(5) Kirsch De Mesmaeker, A.; Lecomte, J. P.; Kelly, J. M. *Top. Curr. Chem.* **1996**, *177*, 25–76.
(6) Elias, B.; Kirsch De Mesmaeker, A. *Coord. Chem. Rev.* **2006**, *250*, 1627–1641.
(7) Turro, N. J.; Barton, J. K.; Tomalia, D. A. *Acc. Chem. Res.* **1991**, *24*, 332–340.
(8) Hage, R.; Prins, R.; Hassnoot, J. G.; Reedijk, J. *J. Chem. Soc., Dalton Trans.* **1987**, 1389–1395.
(9) Hartshorn, R. M.; Barton, J. K. *J. Am. Chem. Soc.* **1992**, *114*, 5919–5925.
(10) Foxon, S. P.; Metcalfe, C.; Adams, H.; Webb, M.; Thomas, J. A. *Inorg. Chem.* **2007**, *46*, 409–416.
(11) Hiort, C.; Lincoln, P.; Norden, B. *J. Am. Chem. Soc.* **1993**, *115*, 3448–3454.
(12) Haq, I.; Lincoln, P.; Suh, D.; Norden, B.; Chowdhry, B. Z.; Chaires, J. B. *J. Am. Chem. Soc.* **1995**, *117*, 4788–4796.
(13) Lincoln, P.; Broo, A.; Norden, B. *J. Am. Chem. Soc.* **1996**, *118*, 2644–2653.
(14) Phillips, T.; Haq, I.; Meijer, A. J. H. M.; Adams, H.; Soutar, A. I.; Swanson, L.; Sykes, J. M.; Thomas, J. A. *Biochemistry* **2004**, *43*, 13657–13665.
(15) Malina, J.; Hennon, M. J.; Brabec, V. *Chem.—Eur. J.* **2008**, *14*, 10408–10414.
(16) Pyle, A. M.; Rehmann, J. P.; Meshoyrer, R.; Kumar, C. V.; Turro, N. J.; Barton, J. K. *J. Am. Chem. Soc.* **1989**, *111*, 3051–3058.
(17) Ossipov, D.; Pradeepkumar, P. I.; Holmer, M.; Chattopadhyaya, J. *J. Am. Chem. Soc.* **2001**, *123*, 3551–3562.
(18) Battacharya, P. K.; Barton, J. K. *J. Am. Chem. Soc.* **2001**, *123*, 8649–8656.

Published on Web 05/11/2010

Scheme 1. Structures of bxbg and Various Polypyridyl Ligands Used in the Present Study

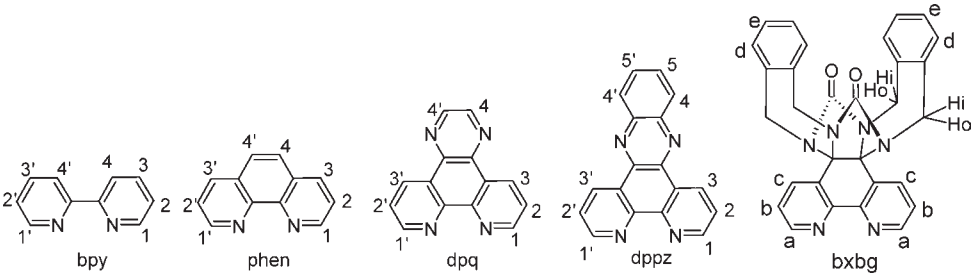

plays a key role in the spectral properties and interaction with DNA.[19−22] Adding groups to the periphery of the ruthenium polypyridyl complexes further expands the functionality of these complexes. For example, insertion of two polyamine tridentate arm-like segments in a macrochelating ligand in the complex $[Ru(dip)_2(macro)]^{n+}$ (dip = 4,7-diphenyl-1,10-phenanthroline, macro = 4,7 $[(NH_2CH_2CH_2)_2NCH_2CH_2NHSO_2C_6H_4]$-1,10-phenanthroline) enables binding of certain divalent metal cations so as to deliver its coordinated nucleophile to the phosphate backbone for hydrolysis of the anionic diester.[23] In a previous study we have explored the possibility of modifying reactivity by using a urea-fused bipyridine ligand (bpg) that contains hydrogen bond donor (N−H) and acceptor (C═O) groups. This ligand is capable of forming extensive H-bonding networks resulting in diverse frameworks encapsulating water/solvent molecules depending upon the number of bipyridine-glycoluril ligands.[24−26] We have also demonstrated that the urea groups of the bpg ligand are involved in DNA binding and facilitate hydrolytic cleavage of DNA.[27] As a part of the program to investigate the DNA-binding properties of ruthenium(II) complexes with bis(*o*-xylene)bipyridine glycoluril, four ruthenium(II) complexes, $[Ru(bpy)_2(bxbg)]Cl_2$ (**1**), $[Ru(phen)_2(bxbg)]Cl_2$ (**2**), $[Ru(dpq)_2(bxbg)]Cl_2$ (**3**), $[Ru(dppz)_2(bxbg)]Cl_2$ (**4**), were synthesized and characterized where bxbg is bis(*o*-xylene)-bipyridine glycoluril (Scheme 1).

The single crystal X-ray structure of **2** reveals a head-to-head and tail-to-tail self-association of amphiphilic metallo-host molecules instead of head to head and head to tail type of self-association of similar molecules in solution state reported by Nolte et al. by NMR dilution and molecular modeling studies.[28−30] The redox reactions of these complexes were investigated by electrochemical and spectroelectrochemical measurements. The interactions of these complexes with DNA were explored by electronic absorption, steady-state, and time-resolved luminescence, luminescence quenching, viscosity, and thermal melting measurements.

Experimental Section

Chemicals. All chemicals and solvents were purchased commercially and were used as received. 1,2-Bis(bromomethyl)-benzene was purchased from Merck India Pvt. Ltd. $RuCl_3 \cdot 3H_2O$ and $K_4[Fe(CN)_6]$ were purchased from S. D. Fine chemicals, Mumbai (India), and calf thymus DNA was purchased from SRL, Kolkata (India) and used as received.

Syntheses. The ligands 1,10-phenenthroline-5,6-dione (phendione),[31] dipyrido[3,2-*d*:2′,3′-*f*]quinoxaline (dpq),[32] and dipyrido-[3,2-*a*:2′,3′-*c*]phenazine (dppz),[33] [4*b*,5,7,7*a*-tetrahydro-4*b*,7*a*-epiminomethanoimino-6*H*-imidazo[4,5-*f*] [1,10] phenanthroline-6,13-dione] (bpg)[24,34] were synthesized according to the literature. The precursor complexes of the type *cis*-$[Ru(N-N)_2Cl_2]$[35,36] are prepared according to the literature method.

Synthesis of bis(*o*-xylene)bipyridine glycoluril (bxbg). This ligand was prepared according to the literature method,[28−30] and the separation was modified as follows. The reaction mixture was poured into 300 mL of water, product was extracted with chloroform (3 × 100 mL), and the combined organic layers were washed with water and then dried ($MgSO_4$). After filtration and rotary evaporation, the residue was purified by column chromatography (SiO_2, $CHCl_3$/MeOH 25:1). Yield: 480 mg (56%). ^{1}H NMR (DMSO-d_6, 300 MHz, 25 °C): δ = 8.88 (2H, d, Hc, J=3.6), 8.74 (2H, d, Ha, J=7.8), 7.54 (2H, dd, Hb, J=4.5, J=3.6), 7.23 (Br, 4H, He), 7.18 (Br, 4H, Hd), 4.96 (4H, NCH_2Ar in J = 16.8), 4.7 (4H, NCH_2Ar out, J = 16.8); IR (KBr pellet, cm^{-1}): ν = 3061, 3012 (ArH), 2951, 2860 (CH_2), 1710 (C═O), 1579, 1564, 1462, 1410 (C═C, C═N); ESI-MS (*m*/*z*, (%) positive mode): 499.2 $(M+H)^+$ (100), Anal. Calcd for $C_{30}H_{22}N_6O_2 \cdot 0.75CHCl_3$; C, 62.80; H, 3.89; N, 14.29; found: C, 62.90; H, 4.08; N, 14.09.

$[Ru(bpy)_2(bxbg)]Cl_2$ (1). The precursor complex *cis*-$[Ru(bpy)_2Cl_2] \cdot 2H_2O$ (100 mg, 0.0192 mmol) and bxbg (96 mg, 0.0192 mmol) were dissolved in methanol−water (1:1, 50 mL), and the mixture was heated to reflux for 8 h, whereupon the color of the solution changed from dark purple to red. The red solution was filtered hot and was cooled to room temperature. The solvent was removed under vacuum to obtain a red solid. The product was purified by column chromatography on active

(19) Xiong, Y.; Ji, L.-N. *Coord. Chem. Rev.* **1999**, *185*, 711–733.
(20) Mei, J. W.; Liu, J.; Zheng, K. C.; Lin, J. Li.; Chao, H.; Li, X. An.; Yun, C. F.; Ji, L.-N. *Dalton Trans.* **2003**, *27*, 1352–1359.
(21) Liu, J.-G.; Zhang, Q.-L.; Shi, X.-F.; Ji, L.-N. *Inorg. Chem.* **2001**, *40*, 5045–5050.
(22) Mariappan, M.; Maiya, B. G. *Eur. J. Inorg. Chem.* **2005**, 2164–2173.
(23) Basile, L. A.; Raphael, A. L.; Barton, J. K. *J. Am. Chem. Soc.* **1987**, *109*, 7550.
(24) Deshpande, M. S.; Kumbhar, A. S.; Puranik, V. G.; Selvaraj, K. *Cryst. Growth Des.* **2006**, *6*, 743–748.
(25) Deshpande, M. S.; Kumbhar, A. S.; Puranik, V. G. *Cryst. Growth Des.* **2008**, *8*, 1952–1960.
(26) Kumbhar, A. S.; Deshpande, M. S.; Butcher, R. J. *CrystEngComm.* **2008**, *10*, 1520–1523.
(27) Deshpande, M. S.; Kumbhar, A. S.; Kumbhar, A. A. *Inorg. Chem.* **2007**, *46*, 5450–5452.
(28) Elemans, J. A. A. W.; Rowan, A. E.; Nolte, R. J. M. *J. Am. Chem. Soc.* **2002**, *124*, 1532–1540.
(29) Elemans, J. A.A.W.; Gelder, R. D.; Rowan, A. E.; Nolte, R. J. M. *Chem. Commun.* **1998**, 1553–1554.
(30) Reek, J. N. H.; Kros, A.; Nolte, R. J. M. *Chem. Commun.* **1996**, 245–247.
(31) Yamada, M.; Tanaka, Y.; Yoshimoto, Y.; Kuroda, S.; Shimao, I. *Bull. Chem. Soc. Jpn.* **1992**, *65*, 1006–1011.
(32) Collins, J. G.; Sleeman, A. D.; Aldrich-Wright, J. R.; Greguric, L.; Hambley, T. W. *Inorg. Chem.* **1998**, *37*, 3133–3141.
(33) Dickerson, J. E.; Summers, L. A. *Aust. J. Chem.* **1970**, *23*, 1023–1027.
(34) Kurth, D. G.; Fromm, K. M.; Lehn, J.-M. *Eur. J. Inorg. Chem.* **2001**, 1523–1526.
(35) Sullivan, B. P.; Salmon, D. J.; Meyer, T. J. *Inorg. Chem.* **1978**, *17*, 3334–3341.
(36) Sprintschnik, G.; Sprintschnik, H. W.; Kirsch, P. P.; Whitten, D. G. *J. Am. Chem. Soc.* **1977**, *99*, 4947–4954.

alumina using acetone and methanol as eluent. The red fraction was collected and concentrated in vacuum to get the pure product. Yield: 131 mg (70%). ^{1}H NMR (DMSO-d_6, 300 MHz, 25 °C); δ = 9.08 (d, 2H, Hc, J = 8.1), 8.86 (d, 4H, H-3′ and H-3, J = 8.1), 8.19 (m, 4H, H-4′ and H-4), 7.88 (d, 4H, Ha and H-1′, J = 5.1), 7.67 (d, 2H, H-1, J = 4.8), 7.56 (6H, m, H-2′, Hb, and H-2), 7.25 (br, m, 4H, He), 7.17 (br, m, 4H, Hd), 5.1 (d, 2H), 4.86 (d, 4H), 4.6 (d, 2H). IR (KBr pellet, cm^{-1}) ν = 3412 (H_2O), 3052, 3020 (ArH), 2949, 2862 (CH2), 1710 (C═O), 1579, 1566, 1458, 1425 (C═C, C═N), ESI-MS (m/z, (%) positive mode): 947 ([M − Cl]$^+$) (∼7%), 456 ([M − 2Cl]$^{2+}$) (∼100%). Anal. Calcd for $C_{50}H_{38}N_{10}O_2Cl_2Ru \cdot 5H_2O$ C, 55.97; H, 4.51; N, 13.05; found: C, 56.23; H, 4.78; N, 12.82.

[Ru(phen)$_2$(bxbg)]Cl$_2$ (2). The synthesis and purification of compound **2** was similar to that of **1** using [Ru(phen)$_2$Cl$_2$]·2H$_2$O (100 mg, 0.0176 mmol) and bxbg (87 mg, 0.0176 mmol). Yield: 139 mg (77%). Crystals were grown by slow evaporation of perchlorate salt of complex which was synthesized by redissolving purified product in water; to that aqueous solution of sodium perchlorate was added the bright red precipitate formed, was collected by filtration, and washed with diethylether. ^{1}H NMR (DMSO-d_6, 300 MHz, 25 °C); δ = 8.99 (d, 2H, Hc, J = 7.5), 8.79 (d, 2H, H-3′, J = 7.2), 8.66 (d, 2H, H-3, J = 8.4), 8.29 (m, 6H, H-4, H-4′ and H-1′), 7.93 (m, 2H, H-2′), 7.83 (m, 4H, H-1, and Ha), 7.64 (m, 2H, H-2), 7.44 (m, 2H, Hb), 7.18 (br, m, 4H, He), 7.13 (br, m, 4H, He), 5.09 (d, 2H), 4.82 (d, 4H), 4.58 (d, 2H); IR (KBr pellet, cm^{-1}); ν = 3398 (H_2O), 3082, 3061 (ArH), 2947, 2843 (CH2), 1712(C═O), 1586, 1492, 1458, 1429 (C═C, C═N). ESI-MS: (m/z, (%) positive mode): 995 ([M − Cl]$^+$) (∼7%), 480 ([M − 2Cl]$^{2+}$) (∼100%). Anal. Calcd for $C_{54}H_{38}N_{10}O_2Cl_2Ru \cdot 3.5H_2O$ C, 59.28; H, 4.14; N, 12.81; found: C, 59.52; H, 4.37; N, 12.62.

[Ru(dpq)$_2$(bxbg)]Cl$_2$ (3). The synthesis and purification of compound **3** was similar to that of **1** using [Ru(dpq)$_2$Cl$_2$]·2H$_2$O (100 mg, 0.0148 mmol) and bxbg (74 mg, 0.0148 mmol); ethylene glycol was used instead of water−methanol mixture. Yield: 101 mg (60%). ^{1}H NMR (DMSO-d_6, 300 MHz, 25 °C); δ = 9.59 (d, 2H, H-3′, J = 8.4), 9.48 (d, 2H, H-3, J = 8.4), 9.33 (d, 4H, H-4, H-4′, J = 5.1), 9.05 (m, 2H, Hc), 8.48 (d, 2H, H-1′, J = 5.1), 8.12 (m, 4H, H-1, H-2′), 7.95 (d, 2H, Ha, J = 7.2), 7.85 (m, 2H, H-2), 7.44 (q, 2H, Hb, J = 8.4, J = 6.3), 7.22 (br, 4H, He), 7.16 (br, 4H, Hd), 5.05 (d, 2H), 4.84 (d, 4H), 4.59 (d, 2H); IR (KBr pellet, cm^{-1}); ν = 3390 (H_2O), 3078, 3061 (ArH), 2941, 2870 (CH_2), 1712 (C═O), 1577, 1518, 1462, 1435 (C═C, C═N); ESI-MS (m/z, (%) positive mode): 1099 ([M − Cl]$^+$) (∼10%), 532 ([M − 2Cl]$^{2+}$) (∼100%). Anal. Calcd for $C_{58}H_{38}N_{14}O_2Cl_2Ru \cdot 4H_2O$ C, 57.71; H, 3.84; N, 16.24; found: C, 57.37; H, 3.98; N, 15.92.

[Ru(dppz)$_2$(bxbg)]Cl$_2$ (4). The synthesis and purification of compound **4** was similar to that of **1** using [Ru(dppz)$_2$Cl$_2$]·2H$_2$O (100 mg, 0.0129 mmol) and bxbg (64 mg, 0.0129 mmol); ethylene glycol was used instead of water−methanol mixture. Yield: 79 mg (50%). ^{1}H NMR (DMSO-d_6, 300 MHz, 25 °C): δ = 9.71 (d, 2H, H-3′, J = 7.2), 9.61 (m, 2H, H-3), 9.07 (d, 2H, Hc, J = 8.4), 8.46 (m, 4H, H-1′, H-5′), 8.33 (d, 2H, H-1, J = 13.8), 8.15 (m, 6H, H-4′, H-5, H-2′), 8.03 (d, 2H, J = 4.8, Ha), 7.88 (m, 4H, H-4, H-2), 7.48 (q, 2H, Hb), 7.23 (br, 4H, He), 7.16 (br, 4H, Hd), 5.09 (d, 2H), 4.88 (d, 4H), 4.61 (d, 2H); IR (KBr pellet, cm^{-1}): ν = 3389 (H_2O), 3080, 3061 (ArH), 2941, 2870 (CH_2), 1714 (C═O), 1582, 1518, 1462, 1423 (C═C, C═N): ESI-MS (m/z, (%) positive mode): 1199 ([M − Cl]$^+$) (∼5%), 582 ([M − 2Cl]$^{2+}$) (∼100%). Anal. Calcd for $C_{66}H_{42}N_{14}O_2Cl_2Ru \cdot 3H_2O$ C, 61.49; H, 3.75; N, 15.21; found: C, 61.27; H, 4.08; N, 14.82.

Caution! *Perchlorate salts of metal complexes with organic ligands are potentially explosive, only small amounts of material should be prepared, and these should be handled with great care.*

Methods and Instrumentation

Spectroscopy and Electrochemistry. ^{1}H NMR spectra were measured on a Varian-Mercury 300 MHz spectrometer with chloroform (d_1) and DMSO (d_6) as a solvent at room temperature, and all chemical shifts are given relative to TMS. Correlation spectroscopy (COSY) and Nuclear Overhauser Effect Spectroscopy (NOESY) spectra of complexes were recorded on a BRUKER 500 MHz spectrometer. The infrared spectra of solid samples dispersed in KBr were recorded on a Shimadzu FTIR-8400 spectrophotometer. Microanalysis (C, H, and N) were carried out with a Thermo Quest microanalysis instrument capable of carrying out C, H, N, S (carbon, hydrogen, nitrogen, and sulfur) analysis. The electrospray mass spectra were recorded on a MICROMASS QUATTRO II triple quadrupole mass spectrometer using water/methanol as solvent. The ESI capillary voltage was set at 3.5 kV, and the cone voltage was 40 V. Microscopy images were captured on FE-SEM (Scanning electron microscope), JEOL, JSM-6360A. UV−vis spectra were recorded on a Jasco UV−vis spectrophotometer in phosphate buffer. Steady-state emission experiments were carried out on a Shimadzu RF-5301 spectrofluorometer at room temperature; the concentration dependent emission spectra's were measured using front face assembly. The emission lifetimes were measured with a time-correlated-single-photon-counting spectrometer from IBH, U.K., using 454 nm nanosecond light emitting diode (NanoLed-01) for the excitation of the sample.

Electrochemical and spectroelectrochemical experiments of ruthenium(II) polypyridyl complexes in acetonitrile solution were performed on a CH-electrochemical analyzer model 1100A with a conventional three-electrode cell assembly with a saturated Ag/AgCl reference electrode, platinum as working electrode, and platinum wire electrode for all measurements in the presence of tetraethyl ammonium perchlorate as supporting electrolyte.

Emission quantum yields (ϕ) were calculated by integrating the area under the luminescence curves and by using eq 1[37] where OD is optical density of the compound at the excitation wavelength (450 nm) and A is the area under the emission spectral curve. The standard used for the luminescence quantum yield measurements was [Ru(bpy)$_3$]Cl$_2$.[38]

$$\phi_{\text{Sample}} = \{\text{OD}_{\text{Standard}} \times A_{\text{Sample}}\}/\{\text{OD}_{\text{Sample}} \times A_{\text{Standard}}\} \times \phi_{\text{Standard}} \quad (1)$$

X-ray Crystallography. A crystal of complex **2** with perchlorate anion suitable for single-crystal X-ray diffraction with a size of 0.4 × 0.2 × 0.02 mm^3 was selected. The data was collected on an Xcalibur-S diffractometer (Oxford Diffraction) using Mo−K$_\alpha$ radiation and ω-scan rotation. Data reduction was performed with CrysAlis Pro,[39] and analytical numeric absorption corrections using a multifaceted crystal model based on an expression derived by Clark and Reid.[40] The structure was solved by direct methods, and the refinement of all non-hydrogen atoms was performed with SHELX97.[41] H atoms are calculated on idealized positions. Structure figures were generated with ORTEP[42] and DIAMOND-3.[43] CCDC 736729 contains the supplementary crystallographic data for **2**. The data can be obtained free of charge via www.ccdc.cam.ac.uk/conts/retrieving.html (or from the Cambridge Crystallographic Data Centre, 12 Union Road, Cambridge CB2 1EZ, U.K.;

(37) Lakowicz, J. R. *Principles of Luminescence Spectroscopy*, 3rd ed.; Springer: New York, 2006.
(38) Caspar, J. V.; Meyer, T. J. *J. Am. Chem. Soc.* **1983**, *105*, 5583–5590.
(39) *CrysAlis Pro, Data collection and data reduction software package*; Oxford Diffraction Ltd.: Abingdon, U.K.
(40) Clark, R. C.; Reid, J. S. *Acta Crystallogr.* **1995**, *A51*, 887–897.
(41) SHELX97 [Includes SHELXS97, SHELXL97]: Sheldrick, G. M., *SHELX97. Programs for Crystal Structure Analysis(Release 97−2)*, University of Göttingen, Germany, 1997.
(42) *ORTEP3 for Windows*; Farrugia, L. J. *J. Appl. Crystallogr.* **1997**, *30*, 565.
(43) Brandenburg, K. *DIAMOND 3*; Crystal Impact GbR: Bonn, Germany.

Table 1. Crystal Data and Structure Refinement for **2**

formula weight	1250.48 g·mol^{-1}
temperature	130(2) K
wavelength	0.71073 Å
crystal system	monoclinic
space group	*C*2/c
unit cell dimensions	a = 44.869(2) Å
	α = 90°
	b = 11.5791(4) Å
	β = 99.800(4)°
	c = 20.9216(7) Å
	γ = 90°
volume	10711.0(7) Å^3
Z	8
density (calcd)	1.551 Mg/m^3
absorption coefficient	0.469 mm^{-1}
F(000)	5134
crystal size	0.35 × 0.22 × 0.03 mm^3
θ range for data collection	2.63 to 24.71°
index ranges	$-52 \le h \le 50$
	$-13 \le k \le 13$
	$-24 \le l \le 24$
reflections collected	40811
independent reflections	9124 [R(int) = 0.1144]
completeness of θ = 24.71°	99.7%
absorption correction	analytical
max. and min transmission	0.985 and 0.875
refinement method	full-matrix least-squares on F^2
restraints/parameters	14/744
goodness-of-fit on F^2	0.795
final R indices [$I > 2\sigma(I)$]	R1 = 0.0512, wR2 = 0.1009
R indices (all data)	R1 = 0.1385, wR2 = 0.1115
largest diff. peak and hole	0.691 and −0.545 e Å^{-3}

fax: (+44)1223−336−033; or deposit@ccdc.cam.uk). Crystal parameters and details of the data collection and refinement are given in Table 1. Selected bond lengths and bond angles are given in Table 2.

DNA Binding Studies. The concentration of CT-DNA was calculated from its known extinction coefficient at 260 nm (6600 M^{-1} cm^{-1}). Solutions of calf thymus DNA in phosphate buffer gave a ratio of UV absorbance at 260 and 280 nm, A_{260}/A_{280} of 1.8−1.9 indicating that the DNA was sufficiently free of protein.

Absorption titration experiments were performed by maintaining a constant metal complex concentration (10 μM) and varying nucleotide concentration (0−60 μM) in buffer. After addition of DNA to the metal complex, the resulting solution was allowed to equilibrate at 25 °C for 20 min, after which absorption readings were noted. The data were then fit to eq 2[44] to obtain intrinsic binding constant K_b.

$$[\mathrm{DNA}]/[\varepsilon_a - \varepsilon_f] = [\mathrm{DNA}]/[\varepsilon_b - \varepsilon_f] + 1/K_b[\varepsilon_b - \varepsilon_f] \qquad (2)$$

Where [DNA] is the concentration of DNA in base pairs, ε_a is the extinction coefficient observed for the MLCT absorption band at the given DNA concentration, ε_f is the extinction coefficient of the complex free in solution, and ε_b is the extinction coefficient of the complex when fully bound to DNA. A plot of [DNA]/[$\varepsilon_a - \varepsilon_f$] versus [DNA] gave a slope 1/[$\varepsilon_a - \varepsilon_f$] and Y intercept equal to 1/K_b [$\varepsilon_b - \varepsilon_f$], respectively. The intrinsic binding constant K_b is the ratio of the slope to the intercept.[44]

Viscosity experiments were carried out using a semimicro viscometer maintained at 28 °C in a thermostatic water bath. Flow time of solutions in phosphate buffer (pH 7.2) was recorded in triplicate for each sample, and an average flow time was calculated. Data were presented as $(\eta/\eta^0)^{1/3}$ versus binding ratio, where η is the viscosity of DNA in the presence of complex and η^0 is the viscosity of DNA alone

(44) Wolfe, A.; Shimer, G. H.; Meehan, T. *Biochemistry* **1987**, *26*, 6392–6396.

Table 2. Selected Bond Lengths [Å] and Angles [deg] for **2**

Bond Lengths			
Ru(1)−N(5)	2.040(4)	Ru(1)−N(2)	2.057(4)
Ru(1)−N(4)	2.046(5)	Ru(1)−N(3)	2.054(5)
Ru(1)−N(6)	2.042(4)	Ru(1)−N(1)	2.061(4)
Bond Angles			
N(5)−Ru(1)−N(4)	95.0(2)	N(6)−Ru(1)−N(3)	96,3(2)
N(5)−Ru(1)−N(6)	78.1(2)	N(5)−Ru(1)−N(1)	96.9(2)
N(4)−Ru(1)−N(6)	88.2(2)	N(2)−Ru(1)−N(3)	94.1(2)
N(5)−Ru(1)−N(2)	91.4(2)	N(4)−Ru(1)−N(1)	96.0(2)
N(4)−Ru(1)−N(2)	172.9(2)	N(6)−Ru(1)−N(1)	173.8(2)
N(6)−Ru(1)−N(2)	96.2(2)	N(2)−Ru(1)−N(1)	80.1(2)
N(5)−Ru(1)−N(3)	172.7(2)	N(3)−Ru(1)−N(1)	88.8(2)
N(4)−Ru(1)−N(3)	79.8(2)		

DNA melting experiments were carried out by monitoring the absorption at 260 nm of CT-DNA (100 μM) with a JASCO V-630 spectrophotometer equipped with a Peltier temperature-controlling programmer ETC-717 (±0.1 °C) in phosphate buffer at various temperatures in the presence and absence of the complexes. UV melting profiles were obtained by scanning A_{260} absorbance monitored at a heating rate of 1 °C/min for solutions of CT-DNA (100 μM) in the absence and presence of ruthenium(II) complexes (20 μM) from 30 to 90 °C with the use of the thermal melting program. The melting temperature T_m which is defined as the temperature where half of the total base pairs is unbound was determined from the midpoint of the melting curves.

Emission titration experiments were performed by using a fixed metal complex concentration to which increments of the stock DNA solutions were added. The typical concentration of metal complex used was 20 μM, and [DNA]/[Ru] ratios ranged between 0 and 30. After the addition of DNA to the metal complex, the resulting solution was allowed to equilibrate for 20−30 min at room temperature before being excited in their intense metal to ligand charge-transfer band between 400 and 500 nm, and emission was measured at 550−750 nm. The excitation and emission slit widths employed were 5 nm each.

Steady-state quenching experiments were conducted by adding 75−750 μL aliquots of a 4 mM ferrocyanide stock solution to 3 mL sample solutions containing 0.8 mM nucleic acid concentration and 20 μM ruthenium(II) complex concentration in phosphate buffer. All solutions were allowed to equilibrate thermally for ∼15 min before measurements were made. Stern−Volmer quenching constant is calculated according to the classical Stern−Volmer eq 3.[37,45]

$$I_0/I = 1 + K_{sv}[\mathrm{Q}] \qquad (3)$$

Where I_0 and I are the luminescence intensities of the complex in the absence and presence of $[Fe(CN)_6]^{4-}$, and K_{sv} is the Stern−Volmer quenching constant which is a measure of the efficiency of luminescence quenching by $[Fe(CN)_6]^{4-}$.

For time-resolved single photon counting measurements the samples were excited in their MLCT band between 400 and 500 nm. Emission was detected in the wavelength range of 550−700 nm depending on the sample, using a photomultiplier tube based detection module (model TBX-04 from IBH). The instrument response function for the present setup is ∼1.2 ns (fwhm: full width half-maximum). The decay curves were analyzed by a reconvolution procedure, using the DAS-6 software, obtained from IBH, considering a suitable functional form (mono- or biexponential) of the decays. The quality of the fits was judged by the reduced chi-square (χ^2) values and the distribution of the weighted residuals among the data channels.

(45) Lakowicz, J. R.; Webber, G. *Biochemistry* **1973**, *12*, 4161–4170.

Scheme 2. Synthetic Route for Complexes **1**−**4**

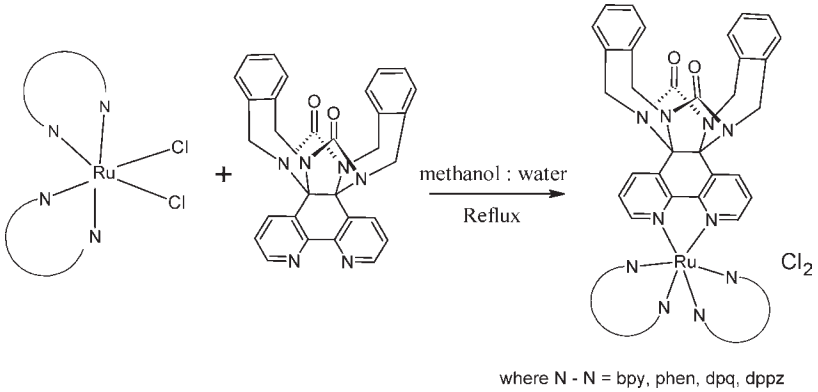

For good fits the χ^2 values were close to unity and the weighted residuals were distributed randomly among the data channels.[46]

Results and Discussion

Syntheses and Characterization. Bis(*o*-xylene)bipyridine glycoluril (bxbg) was synthesized by alkylation of bipyridine glycoluril with 1,2-bis(bromomethyl)benzene in dimethyl sulphoxide with KOH as a base in good yield (56%). Its composition was determined by elemental analysis, ^{1}H NMR, COSY, IR spectroscopy, and mass spectrometry (see Experimental Section). The corresponding ruthenium(II) polypyridyl complexes of the type $[Ru(N-N)_2(bxbg)]Cl_2$ (**1**−**4**) were synthesized as shown in Scheme 2 by reacting bxbg with appropriate precursors followed by chromatographic purification using neutral alumina column and obtained as racemic mixtures. The perchlorate salt of the complex was synthesized by adding aqueous sodium perchlorate solution to the aqueous solution of the purified product, and the bright red precipitate formed was collected by filtration and washed with diethylether. The compounds were characterized by NMR, IR, elemental analysis, electrochemistry, UV−visible spectroscopy, and electrospray mass spectrometry (see Experimental Section). In ESI-MS, peaks due to $[M - Cl]^+$ and $[M - 2Cl]^{2+}$ were observed.

Crystal Structure. Single crystals suitable for X-ray diffraction were grown by slow evaporation of perchlorate salt of complex **2** in acetonitrile and water mixture at room temperature. The compound crystallizes in the monoclinic space group *C*2/*c*. A summary of the crystallographic data, bond lengths, and bond angles for **2** are given in Table 1 and 2. An ORTEP representation of the cation of **2** is shown in Figure 1A. The ruthenium(II) ion is chelated by the bxbg ligand and two phenanthroline ligands oriented in a cis geometry. The coordination geometry around Ru1 is best described as distorted octahedral, with an average bite angle of 79.42° for the three bidentate ligands. The distortion from an ideal octahedral geometry is due to the narrow bite angles of the phenanthroline moieties as observed in some other ruthenium polypyridyl complexes.[47−49] The mean Ru−N (phen) bond length is 2.050 Å, and the Ru−N (bxbg) bond length of 2.040 Å is similar to that found in other analogous mixed ligand polypyridyl ruthenium complexes.[24,25,50]

Molecular packing shows a "head-to-head" and "tail-to-tail" self-association of the molecules (Figure 1B). Such a behavior is observed for amphiphilic molecules, containing hydrophobic head groups and hydrophilic tails. These molecules form self-assembled structures in solution at higher concentration to maximize the interaction of the hydrophilic part with the solvent, while minimizing the contact of the hydrophobic part with the solvent.[30]

There are weak intermolecular CH···O contacts detectable between H(36)···O(1) = 2.508(4) Å and H(34)···O(2) = 2.344(4) Å. These interactions may be responsible for the unexpected "head-to-head" configuration of the complex molecules. As illustrated in Figure 1C there are no interactions between the aromatic pi systems of the bxbg-ligands because the pi electrons of the aromatic ring systems are not pointing toward each other.

Taking these weak intermolecular hydrogen bonds into account a two-dimensional layer in [0,1,1] parallel to the a-face of the unit cell is formed. These layers are packed on top of each other along the *a*-axis together with the perchlorate anions. Between these layers the phen-ligands are configured in a "tail-to-tail" fashion. A analysis of this molecular arrangement reveal voids through the entire structure along the *b* axis (Figure 1D). Although the crystals have been grown from an acetonitrile/water mixture, these channels are occupied by diethyl ether and water molecules because the crystals were isolated and stored in diethyl ether. Apparently diethyl ether had completely replaced all originally housed acetonitrile molecules. This also indicates that the solvent molecules are easily accessible and exchangeable by other small molecules

Photophysical Studies. The photophysical properties of complexes **1**−**4** are summarized in Table-3. The UV−Visible spectra of **1**−**4** recorded in phosphate buffer solution are dominated by high-energy bands between 240 to 300 nm which corresponds to $\pi \rightarrow \pi^*$ transitions of the

(46) O'Connor, D. V.; Phillips, D. *Time Correlated Single Photon Counting*; Academic Press: New York, 1984; Vol. *99*, p 4947.
(47) Santra, B. K.; Menon, M.; Pal, C. M.; Lahiri, G. K. *J. Chem. Soc., Dalton Trans.* **1997**, 1387–1393.
(48) Xiong, Y.; He, X.-F.; Zou, X.-H.; Wu, J- Z.; Chen, X.-M.; Ji, L.-N.; Li, R.-H.; Zhou, J.-Y.; Yu, K. B. *J. Chem. Soc., Dalton Trans.* **1999**, 19–23.
(49) Wu, J.-Z.; Ye, B.-H.; Wang, L.; Ji, L.-N.; Zhou, J.-Y.; Li, R.-H.; Zhou, J.-Y. *J. Chem. Soc., Dalton Trans.* **1997**, 1395–1401.
(50) Rillema, D. P.; Jones, D. S.; Woods, C.; Levy, H. A. *Inorg. Chem.* **1992**, *31*, 2935–2938.

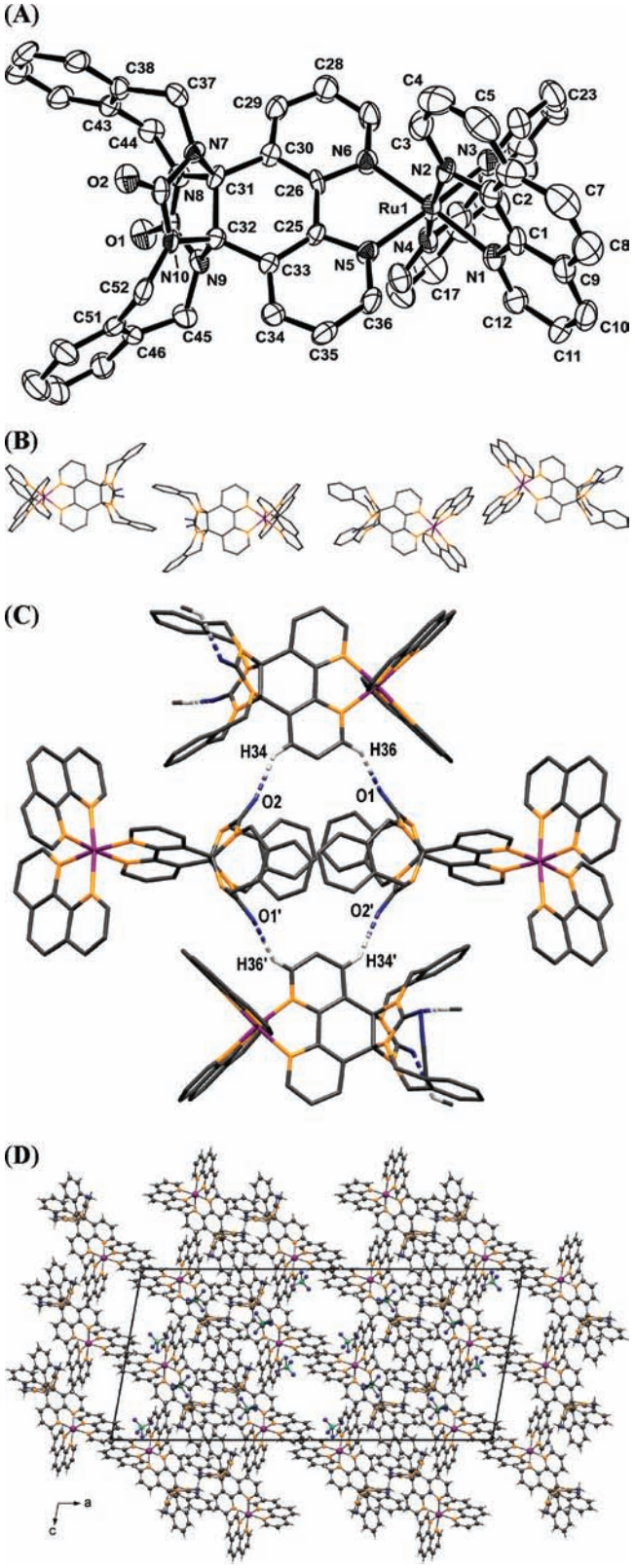

Figure 1. (A) ORTEP of the $[Ru(phen)_2(bxbg)]^{2+}$ cation ($(ClO_4)^-$ anions are omitted for clarity). (B) Head-to-head dimer (left) and tail-to-tail dimer (right). (C) Intermolecular CH···O contacts. (D) Solvent accessible channels along the *b* axis.

aromatic nitrogen donor ligands. The UV−visible spectrum of the dppz-containing complex exhibits a moderately intense band in the near UV region, that is, at 360 nm, which is characteristic of a $\pi \rightarrow \pi^*$ (dppz) transition.[51,52] The low energy bands around 450 nm for **1**−**4** are assigned as the MLCT Ru ($d\pi$) → ligand (π^*) transitions[53,54] typical of polypyridyl ruthenium(II) complexes.

The luminescence of these complexes has been examined in water, in acetonitrile, and in dimethyl formamide (DMF) by excitation into the MLCT band of complexes **1**−**4** at room temperature. All complexes emits brightly in acetonitrile with a characteristic broad emission peak centered between 605 and 640 nm but weakly in water. The complex **4** has very weak luminescence in aqueous buffer solution, but in acetonitrile this complex is highly luminescent compared to other complexes. The emission maxima, lifetimes, and quantum yields with respect to $[Ru(bpy)_3]^{2+}$ as standard were compiled in Table 3

Electrochemistry. Cyclic voltammetry of complexes **1**−**4** were investigated in acetonitrile. The cyclic voltammogram of complex **1** is shown in Figure 2. Although ruthenium(II) complexes exhibit a series of ligand-based reduction processes under voltammetric conditions, the present study reports only details of oxidation of Ru^{II} to Ru^{III}. The series of complexes **1**−**4** shows two oxidation peaks in the range of 0.2 to 1.6 V. The peak at lower potential corresponds to ligand (bxbg) oxidation, and the reversible peak at higher potential corresponds to Ru^{II} to Ru^{III} oxidation. Reversible potentials (E^0_f values) were assumed to be equal to the midpoint potentials (E_m) and were determined from the average of the oxidation (E_p^{ox}) and reduction (E_p^{red}) peak potential, $(E_p^{ox} + E_p^{red})/2$ and reported with respect to $Fc^{0/+}$ as internal standard (Table 4).

As expected the midpoint potential for the Ru^{II}/Ru^{III} redox couple in **1**−**4** is more positive than that of $[Ru(bpy)_3]^{2+}$, in accordance with the extension of the corresponding π framework similar to other ruthenium(II) mixed polypyridyl complexes.[54−56] The differences between peak oxidation and reduction potential are close to that observed for the reversible couple (80 mV) at 100 mV s^{-1}, indicating that these processes are electrochemically reversible one-electron processes. The values of $|I_p^{ox}/I_p^{red}|$ are close to unity as expected for a chemically reversible system.[57]

The reversible potential can be systematically varied through ligand substitution. Increase in electron delocalization in going from complex **1** to **4** gives rise to more positive E_f^0 values.

Spectroelectrochemistry. To further probe the metal-based (Ru^{II}/Ru^{III}) redox process, bulk electrolysis experiments were conducted. For all complexes a constant potential 250 mV higher than that of the oxidation potential (vs Fc/Fc^+) was applied at a platinum gauze electrode to a 30 μM acetonitrile solution, and the oxidation to Ru^{III} in situ

(51) Waterland, M. R.; Gordon, K. C.; McGarvey, J. J.; Jayaweera, P. M. *J. Chem. Soc., Dalton Trans.* **1998**, 609–616.
(52) Lundin, N. J.; Walsh, P. J.; Howell, S. L.; Blackman, A. G.; Gordon, K. C. *Chem.—Eur. J.* **2008**, *14*, 11573–11583.
(53) Freedman, D. A.; Evju, J. K.; Pomije, M. K.; Mann, K. R. *Inorg. Chem.* **2001**, *40*, 5711–5715.
(54) Liu, J. G.; Zhang, Q.-L.; Shi, X.-Fa.; Ji, L.-N. *Inorg. Chem.* **2001**, *40*, 5045–5050.
(55) Juris, A.; Balzani, V.; Barigelletti, F.; Campagna, S.; Belser, P.; Van Zelewski, A. *Coord. Chem. Rev.* **1988**, *84*, 85–277.
(56) Sentagne, C.; Chambron, J. C.; Sauvage, J. P.; Paillous, N. *J. Photochem. Photobiol. B: Biol.* **1994**, *26*, 165–174.
(57) Nickita, N.; Gasser, G.; Pearson, P.; Belousoff, M. J.; Goh, Lai Y.; Bond, A. M.; Deacon, G. B.; Spiccia, L. *Inorg. Chem.* **2009**, *48*, 68–81.

Table 3. Photophysical Data for Ruthenium(II) Polypyridyl Complexes **1**−**4**

	absorbance λ_{max} (nm) /ε (M^{-1} cm^{-1})		emission							
	(buffer)		(buffer)				(acetonitrile)		(DMF)	
complexes[a]	ligand transitions	MLCT	λ_{em}(nm)	ϕ_{em}[b]	τ_1	τ_2(ns)[c]	λ_{em}(nm)	ϕ_{em}[b]	λ_{em}(nm)	ϕ_{em}[b]
1	286/41635, 244/20230	446/8130	637	0.010	238		623	0.029	632	0.022
2	386/9100, 262/63695	438/10460	631	0.014	337		614	0.033	622	0.027
3	290/38020, 256/69140	450/15305	613	0.027	109	438	609	0.046	610	0.038
4	360/25190, 280/84400	458/15177	609	0.001	45	181	604	0.068	610	0.054
[d]$[Ru(bpy)_3]^{2+}$			603	0.042			606	0.063	601	0.062

[a] [Ru] = 20 μM. [b] ϕ_{em} = Emission quantum yield. [c] τ_1, τ_2 = Emission lifetime; Error limit: λ_{max} = ± 2 nm, λ_{em} = ± 2 nm, τ = ± 2 ns. [d] Data taken from ref 38.

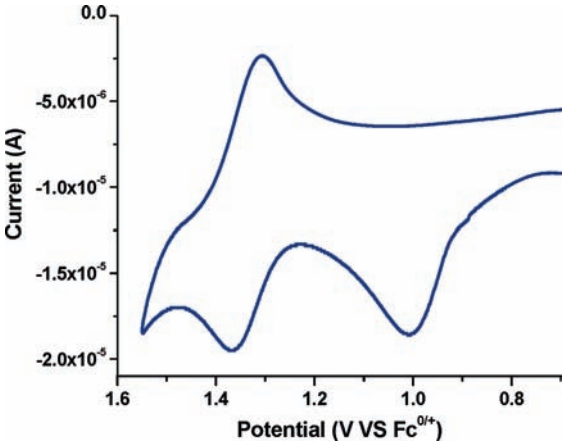

Figure 2. Cyclic voltammogram of **1** in CH_3CN with ferrocene (Fc) as the internal reference.

was monitored by UV−visible spectroscopy. In case of complex **1**, a constant potential of 1140 mV (vs Fc/Fc^+) was applied at a platinum gauze electrode to a 30 μM acetonitrile solution, and the oxidation to Ru^{III} in situ was monitored by UV−visible spectroscopy (Figure 3). In the UV region the band at 285 nm decreased in intensity accompanied by growth of a band at 315 nm. The band at 246 nm increased in intensity, and in the visible region the band at 450 nm decreased in intensity and the oxidized species display a weak band at 430 nm. Isosbestic points were observed at 326, 297, and 269 nm indicating a clean oxidation reaction. After the potential was removed no reconversion to $[Ru^{II}(bpy)_2(bxbg)]^{2+}$ was observed, despite the low concentration of complex used and the very positive potential. However, by altering the potential to 800 mV (vs Fc/Fc^+) complete reversion to $[Ru^{II}(bpy)_2(bxbg)]^{2+}$ was achieved.[57,58] All these data are consistent with the chemically reversible process:

$$[Ru^{II}(bpy)_2(bxbg)]^{2+} \rightleftharpoons [Ru^{III}(bpy)_2(bxbg)]^{3+} + e^-$$

The three bands in the ultraviolet region observed for the electrogenerated Ru^{III} complex at 246 nm and 280, 315 nm have been assigned to intraligand ($\pi \rightarrow \pi^*$) transitions of the polypyridyl ligands.[59,60] The weak band observed in the visible region at 425 nm is attributed to a ligand-to-metal charge transfer (LMCT) transition ($\pi \rightarrow t_2$) characteristic of Ru^{III}.[60]

Table 4. Electrochemical Data

	oxidation potential (E^0_f in V)[a]	
complexes	ligand based	metal based
bxbg	0.60	
$[Ru(bpy)_3]^{2+}$		0.88
1	0.62	0.94
2	0.61	0.95
3	0.62	1.01
4	0.62	1.02

[a] Data reported for 1 mM solutions in CH_3CN with $(Et_4N)ClO_4$ as the supporting electrolyte. Scan rate was 100 mV/S vs Fc/Fc^+, error limit: E^0_f = ± 0.01 V.

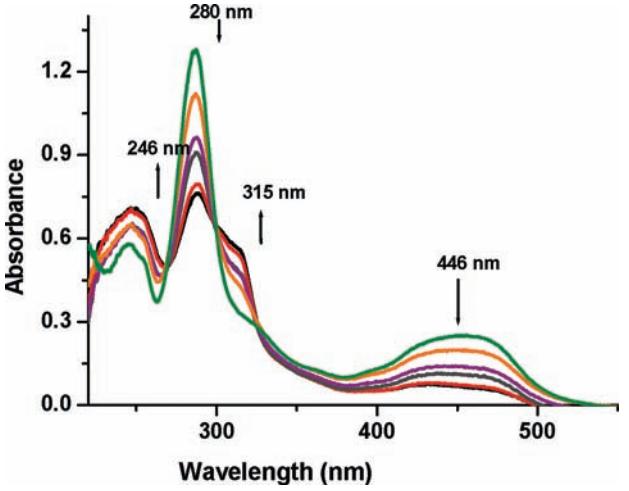

Figure 3. UV−visible spectroelectrochemical responses of **1** (30 μM) in MeCN (0.1 M $(Et_4N)ClO_4$), during oxidation.

Self-Association Studies

NMR Dilution Studies. NMR dilution experiments were carried out in D_2O to investigate the self-association of hydrophobic receptor cavities of complexes in water. For complex **2** concentration dependence of ^1H NMR spectral changes was observed at 25 °C, spectra were recorded at approximately 1, 3, 15 mM concentration (Supporting Information, Figure S12). Several proton resonances in the spectra of **2** were very sensitive to change in concentration. Upon dilution the resonances of sidewall protons Hd, He, exhibit larger shifts (downfield) whereas the resonances of the other protons display only relatively small up- and downfield shifts.

(58) Sherborne, J.; Scott, S. M.; Gordon, K. C. *J. Inorg. Chim. Acta* **1997**, *260*, 199–205.
(59) Bryant, G. M.; Fergusson, J. E. *Aust. J. Chem.* **1971**, *24*, 275–286.
(60) Nazeeruddin, M. K.; Zakeeruddin, S. M.; Kalyanasundaram, K. *J. Phys. Chem.* **1993**, *97*, 9607–9612.

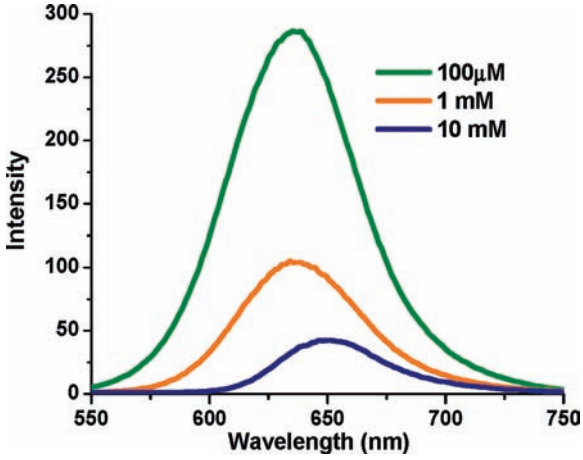

Figure 4. Steady-state emission spectra of complex **1** in water at different concentrations at 298 K.

This suggests the possibility of the formation of a head-to-head self-assembly in aqueous solution. At higher concentration the high field shifts of around 0.6 ppm for the side wall protons H_d; H_e is attributable to the presence of $\pi-\pi$ interaction due to head-to-head association, which is accompanied by broadening of peaks. It is interesting to note that one set of the phenanthroline protons (1, 2, and 3) is relatively more shielded than the other set (1′, 2′, and 3′). To get more insight to the intermolecular association of **2**, we have carried out 2D NOESY measurements at different concentration of compound in D_2O at a mixing time of 750 ms (Supporting Information, Figure S13). The NOEs are expected to be weak as the molecule of interest is of intermediate molecular weight (1029.97) and hence the NOESY cross peaks can either be positive or negative depending on the correlation time. In all the three concentrations studied, we observed positive cross peaks indicating the slow tumbling of the molecule even at the concentration of 1 mM. At concentration of 1 mM only a few relatively weak cross-peaks were observed in comparison to the strong cross peaks in the other two cases. The role of an efficient spin diffusion due to an increase in the correlation time is obvious at 3 mM and 15 mM concentrations which is likely to arise from the intermolecular $\pi-\pi$ association of **2** leading to dimeric or higher molecular assemblies.

Steady-State Luminescence. To investigate the influence of the concentration on the emission spectra, solutions of complex **1** in water varying in concentration from 100 μM to 10 mM were prepared and measured to confirm the formation of aggregates at higher concentration. As the concentration of the complex increased, the quenching of emission intensity was observed to be nearly 7-fold (Figure 4) along with a red shift in emission wavelength of 11 nm on going from 100 μM to 10 mM concentration. Further support for this comes from the fact that emission of complex **1** increased when small quantities of acetone (5%), a solvent known to cause dissociation of the self-assembled structures in water,[30] was added to the solution of the complex. These results indicate that concentration has a drastic effect on the emission spectra indicating excitonic interaction between molecules by head-to-head, tail-to-tail, and head-to-tail association forming aggregates.

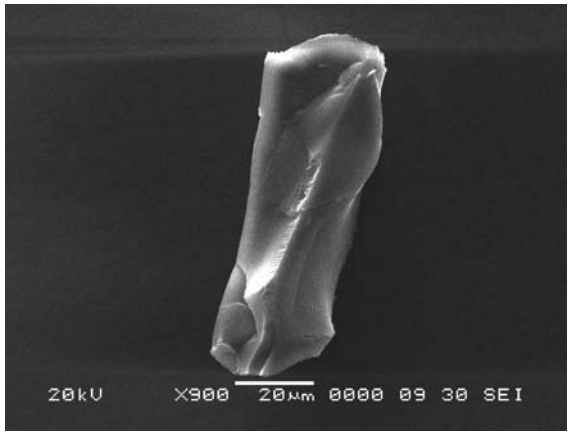

Figure 5. SEM image of **2**.

Electron Microscopy Studies. The aggregate formation by the self-association of the hydrophobic receptor cavities of **2** in water was investigated by scanning electron microscopy (SEM). SEM images obtained 1 day after sample preparation showed rod-like and rectangular aggregates observed for complex **2** (Figure 5 and Supporting Information, Figure S14)

The X-ray powder diffraction of dried aqueous samples of all four complexes revealed no clear reflections (Supporting Information, Figure S15). This also implies that the aggregates are built up from molecular units that interact in very diverse ways in a variety of geometries.

On the basis of above-discussed ^{1}H NMR, NOESY, steady state dilution studies, and X-ray powder diffraction studies we can predict that the formation of aggregates takes place by self-association of molecules in water at higher concentration, which was further confirmed by electron microscopy studies.

DNA Binding Studies

Absorption Spectroscopy Studies. Monitoring the effect of adding increasing amounts of DNA on the absorption spectrum of a metal complex is one of the most widely used methods for determining overall binding constants. In general, the hypochromism and red shift are associated with the binding of the complex to the helix because of the interaction between the aromatic chromophore of the complex and the base pairs of the DNA. The magnitude of the hypochromism and red shift depends on the strength of interaction between DNA and the complex.[61−65] The absorption spectra of complexes **3** and **4** in the absence and presence of CT-DNA are given in Figure 6. The absorbance spectra shows clearly that the addition of DNA to the complexes yields hypochromism, associated with a red shift with increasing DNA concentration; for complex **4** the highest hypochromism is about 24.8%, 46.2%, and 55.3%, at 458, 362, 280 nm, respectively, indicating strong binding of this complex

(61) Deshpande, M. S.; Kumbhar, A. A.; Kumbhar, A. S.; Kumbhakar, M.; Pal, H.; Sonawane, U.; Joshi, R. R. *Bioconjugate Chem.* **2009**, *20*, 447–459.
(62) Pellegrini, P. P.; Aldrich-Wright, J. R. *Dalton Trans.* **2003**, 176–183.
(63) Barton, J. K.; Danishshefsky, A. T.; Goldberg, J. M. *J. Am. Chem. Soc.* **1984**, *106*, 2172–2176.
(64) Friedman, A. E.; Kumar, C. V.; Turro, N. J.; Barton, J. K. *Nucleic Acids Res.* **1991**, *19*, 2595–2602.
(65) Pyle, A. M.; Barton, J. K. *Bioinorganic Chemistry*; Wiley: New York, 1990, *38*, 413.

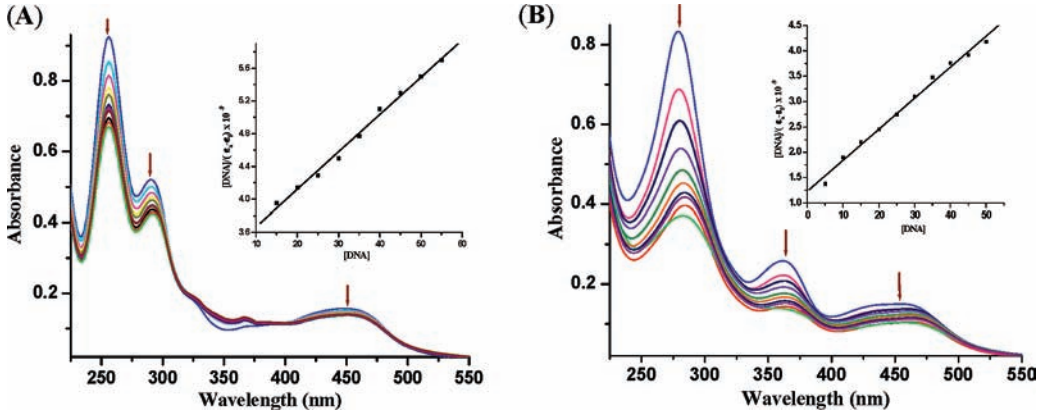

Figure 6. Changes in the electronic absorption spectra of (A) **3** (10 μM), (B) **4** (10 μM) with increasing concentrations (0−60 μM) of CT-DNA (phosphate buffer, pH 7.2); the inset graph shows a fitting of the absorbance data used to obtain the binding constant.

Table 5. Electronic Absorption Data upon Addition of CT-DNA

complexes[a]	$\Delta\lambda_{max}$ (MLCT)	hypochromism H (%)[b]			K_b (M^{-1})
2	2	8.2 (438)	12.2 (386)	14.2 (262)	3.9×10^3
3	4	12.9 (448)	18.5 (290)	27.5 (256)	1.42×10^4
4	8	24.8 (458)	46.2 (362)	55.3 (280)	4.98×10^4
$[Ru(bpy)_2(dppz)]^{2+}$ [c]		14.5 (444)	40.1 (372)		5.0×10^6
$[Ru(phen)_2(dppz)]^{2+}$ [d]			35 (370)		5.1×10^6
$[Ru(NH_3)_4(dppz)]^{2+}$ [e]		13.6 (544)			1.2×10^5

[a] [DNA]/[Ru] = 7:1. [b] H % = $100(A_{free} - A_{bound})/A_{free}$ in phosphate buffer (pH = 7.2) where A = Absorbance; [c] Data taken from ref 66. [d] Data taken from refs 11, 12, 67. [e] Data taken from ref 68. Error limit: λ_{max} = ±2 nm, H (%) = ±5%; K_b (M^{-1}) = ±5%.

compared to other complexes; the percentage of hypochromism and red shift at the MLCT band are listed in Table 5.

To compare quantitatively the binding strength of these complexes, their intrinsic binding constants with CT-DNA were obtained by monitoring the changes in absorption at intraligand band (Figure 6) with increasing concentration of DNA using eq 2 and were found to be 3.9×10^3, 1.42×10^4, and 4.98×10^4 M^{-1} for complex **2**, **3**, and **4**, respectively. This significant difference in DNA binding affinity of complexes **2**−**4** can be understood as a result of the fact that the dppz and dpq ligands display a more conjugate system than the phen ligand. These spectral characteristics suggest that complex **2** interacts with DNA by groove binding and complexes **3**, **4** interact with DNA through a mode that involves a stacking interaction of the planar aromatic chromophore and the base pairs of DNA, but with a moderate binding constant as compared to classical intercalators ($[Ru(phen)_2(dppz)]^{2+}$, $K_b = 5.1 \times 10^6$ M^{-1}) probably because of hindrance to the intercalation by the second planar dpq, dppz, and the nonplanar bxbg ancillary ligand.[61−65]

Steady-State Emission Studies. The changes in the emission spectra of ruthenium(II) polypyridyl complexes in the presence of DNA are diagnostic means to determine the DNA binding.[69,70] The steady-state emission spectra of 20 μM solutions of complexes **1**−**4** in phosphate buffer (pH 7.2) show increase in the emission intensity with successive addition of CT-DNA (Figure 7 and Supporting Information, Figure S16). The spectra profiles and emission maxima for complexes **1** and **2** exhibit weak luminescence enhancements in the range of 1 to 1.4 after adding CT-DNA at a ratio of [DNA]/[Ru] = 30 indicating a weak binding of these complexes with CT−DNA by groove binding or electrostatic association (Table 6). However, complexes **3** and **4** exhibit luminescence enhancement of 2.2 to 3.8 indicating strong binding by intercalation of this complex with CT−DNA consistent with the intercalating mode. The ligands dppz and dpq are expected to insert more deeply and strongly than bpy and phen which results in enhancement in emission intensity. Increase in luminescence intensity is due to two reasons: first, the hydrophobic environment inside the DNA helix reduces the accessibility of water molecules to the complex, and second, the complex mobility is restricted at the binding site and so the vibrational mode of relaxation decreases.[49]

Steady-State Emission Quenching Experiment using $K_4[Fe(CN)_6]$. Steady-state emission quenching experiments using $[Fe(CN)_6]^{4-}$ as quencher can further support the interaction of these complexes with DNA.[71] The results of steady state emission quenching experiments using $[Fe(CN)_6]^{4-}$ as the quencher are shown in the Supporting Information, Figure S17. The results are interpreted in terms of two binding modes: electrostatic, which is easily quenched by ferrocyanide, and intercalative, which is protected from ferrocyanide quenching. Stern−Volmer

(66) Liu, J. G.; Zhang, Q. L.; Shi, X. F.; Ji, L. N. *Inorg. Chem.* **2001**, *40*, 5045–5050.
(67) Friedman, A. E.; Kumar, C. V.; Turro, N. J.; Barton, J. K. *Nucleic Acids. Res.* **1991**, *19*, 2595.
(68) Nair, R. B.; Teng, E. S.; Kirkland, S. L.; Murphy, C. J. *Inorg. Chem.* **1998**, *37*, 139–141.
(69) Jenkins, Y.; Friedman, A. E.; Turro, N. J.; Barton, J. K. *Biochemistry* **1992**, *31*, 10809–10816.
(70) Treadway, J. A.; Loeb, B.; Lopez, R.; Anderson, P. A.; Keene, F. R.; Meyer, T. J. *Inorg. Chem.* **1996**, *35*, 2242–2246.
(71) Elfring, W. H.; Crosby, G. A. *J. Am. Chem. Soc.* **1981**, *103*, 2683–2687.

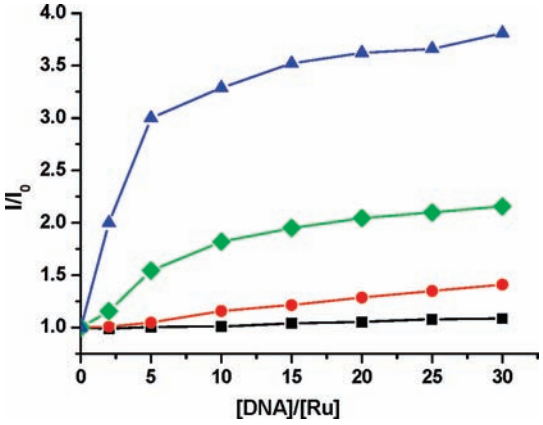

Figure 7. Plots of relative integrated emission intensity versus [DNA]/[Ru] for complexes **1** (black squares), **2** (red circles), **3** (green diamonds), **4** (blue triangles) (20 μM, in phosphate buffer, pH 7.2 at 298 K with increasing [DNA]/[Ru] ratio from 0 to 30.

Table 6. Luminescence and Thermal Properties of Complexes **1**−**4** in the Absence and Presence of CT-DNA

			Stern−Volmer quenching constant (M^{-1})[b]	
complexes	ΔT_m/°C	I/I_0[a]	without DNA	with DNA
1	1	1.06	1.36×10^3	1.04×10^3
2	4	1.4	1.60×10^3	6.5×10^2
3	5	2.2	1.07×10^3	1.4×10^2
4	8	3.8	2.0×10^3	0.78×10^2

[a] Relative emission intensity enhancement in the presence of CT-DNA at [DNA]/[Ru] = 30:1. [b] Stern−Volmer constants for the quenching of the complexes by $K_4[Fe(CN)_6]$ in the absence and presence of DNA.

quenching constants for complexes **1**−**4** in the absence and presence of DNA are given in Table 6. In the absence of DNA, complexes **1**−**4** are efficiently quenched by $[Fe(CN)_6]^{4-}$ with Stern−Volmer quenching constants of the order of $1.07-2.0 \times 10^3$. However, in the presence of DNA, the maximum decrease in the Stern−Volmer quenching constant is obtained for complexes **3** and **4** indicating strong binding of these complexes by intercalation.[48,49] Quenching of this luminescent excited state with the use of an anionic quencher such as $[Fe(CN)_6]^{4-}$ has been shown to be able to distinguish bound ruthenium(II) species.[72] A highly negatively charged quencher is expected to be repelled by the negatively charged phosphate backbone and therefore a DNA-bound cationic molecule should be protected from quenching while the free complexes should be readily quenched.

DNA Melting Experiments. Other evidence for the intercalation of the complexes into the helix was obtained from the DNA melting studies. Intercalation of small molecules into the double helix is known to increase the helix melting temperature (T_m),[73−76] the temperature at which the double helix denatures into single-stranded DNA. The extinction coefficient of DNA bases at 260 nm in the double−strand is much less than in the single-stranded form; hence, melting of the helix leads to increase in the absorption at this wavelength. CT-DNA was seen to melt at 63 ± 1 °C (phosphate buffer) in the absence of complex. The melting temperature of DNA increased by 4, 5, and 8 °C for complexes **2**, **3**, and **4**, respectively, which indicates that complex **4** binds strongly compared to other complexes (Table 6). The increase in melting temperature is lower than classical intercalators, suggesting that the dpq and dppz complexes bind with DNA through a mode that involves a stacking interaction of the planar aromatic chromophore and the base pairs of DNA, but the moderate binding probably because of the influence of ancillary bxbg ligand.

Viscometric Titration. Intercalation of an organic drug or metal complexes into DNA is known to cause a significant increase in viscosity of a DNA solution because of an increase in separation of base pairs at the intercalation site, and hence, an increase in overall DNA molecular length. In contrast, a ligand that binds in the DNA grooves causes less-pronounced changes or no change in viscosity of a DNA solution. The effect of EtBr (ethidium bromide) and complexes on the viscosity of DNA were studied to access the binding mode of complexes with the DNA. Figure 8 shows changes in the viscosity of DNA in the presence of EtBr and complexes. The addition of EtBr to DNA increases the relative viscosity of DNA dramatically which is consistent with intercalation, compared to EtBr increase in viscosity of DNA upon addition of complex **3**, and **4** less indicating partial intercalation, however much smaller increase of viscosity upon addition of complex **1** and **2** indicating groove or electrostatic binding of these complexes.

Time Resolved Emission Measurements in the Presence of DNA. DNA binding of these complexes is further confirmed by time-correlated single photon counting luminescence measurements. The luminescence lifetime of complexes **1**−**4** in the presence and absence of CT-DNA for a ratio [DNA]/[Ru] of 2 to 30 is given in the Supporting Information, Table S1. Complex **2** exhibits monoexponential decay; however, the lifetime increases from 330 to 432 ns. The luminescent characteristics of complexes **3** and **4** bound to DNA shows bi- and triexponential decay in emission indicating the presence of two and three distinguishable DNA binding modes for the complexes. Two binding modes were proposed for complex **3**, one may be partial intercalation while the other is groove-bound interaction or electrostatic interaction in which the excited state lifetime is comparable to that of the free form. When the binding ratio [DNA]/[Ru] is varied from 2:1 to 30:1 for complex **4**, the excited state lifetimes increased from 45 to 182 ns for short lifetime components and from 228 to 747 and 181 to 373 ns for long lifetime components, and for complex **3** from 109 to 200 ns for short lifetime components and from 438 to 800 ns for long lifetime components. The steady-state quenching experiments and time-resolved emission measurements on complex **4** suggest that both long lifetime components could be assigned to partial intercalative binding depending on the orientations of the two dppz ligands in the complex and short lifetime components for

(72) Tysoe, S. A.; Morgan, R. J.; Baker, A. D.; Streakas, T. C. *J. Phys. Chem.* **1993**, *97*, 1707–1711.
(73) Waring, M. J. *J. Mol. Biol.* **1965**, *13*, 269–282.
(74) Kelly, J. M.; Tossi, A. B.; MacConell, D. J.; OhUigin, C. *Nucleic Acids Res.* **1985**, *13*, 6017–6034.
(75) Neyhart, G. A.; Grover, N.; Smith, S. R.; Kalsbeck, W. A.; Fairly, T. A.; Cory, M.; Throp, H. H. *J. Am. Chem. Soc.* **1993**, *115*, 4423–4428.
(76) Long, E. C.; Barton, J. K. *Acc. Chem. Res.* **1990**, *23*, 271–273.

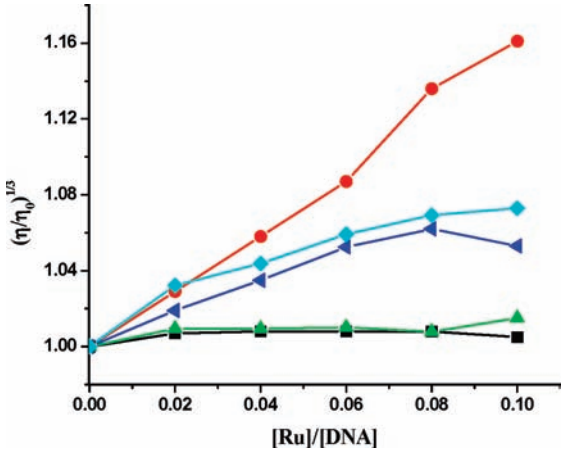

Figure 8. Effect of increasing amount of the EtBr (red circles), Complex **1** (black squares), Complex **2** (green triangles), Complex **3** (blue triangles), and Complex **4** (cyan diamonds) on the relative viscosities of calf thymus DNA at 28.0 °C [DNA] = 300 μM.

a surface-bound mode. The results are also consistent with intercalation and electrostatic binding being the two binding modes.[61]

Conclusions

In the present study we have synthesized a series of new ruthenium(II) polypyridyl complexes containing bis(*o*-xylene)bipyridine glycoluril and characterized them by various physical methods. Electrochemical studies of **1**−**4** showed a reversible Ru^{II}/Ru^{III} oxidation process at 0.94, 0.95, 1.01, 1.02 V (vs Fc/Fc^{+}), respectively. The order of redox potentials **1** < **2** < **3** < **4** indicates an increase in stability of the ruthenium(II) state which mirrors the increased aromaticity of the ligands. X-ray structure packing diagram of **2** shows channels running through the structure partially occupied by solvent molecules and also head-to-head and tail-to-tail self-association of the molecules. Formation of aggregates of complexes by different self-associated species in water was confirmed by ^{1}H NMR, NOESY, and steady-state luminescence dilution experiments at various concentrations. This was further evidenced by electron microscopy studies. The modification of the ancillary bipyridine ligand results in different DNA binding behaviors for complexes **1**−**4**.

Acknowledgment. A.S.K. acknowledges Department of Science and Technology (DST), New Delhi, India, for financial support under "New Initiatives in Bioinorganic chemistry" (SR/S5/BC-25/2006). S.S.B. acknowledges Department of Science and Technology (DST), New Delhi, India, for providing a fellowship under the scheme SR/S5/BC-25/2006. A.S.K. acknowledges University of Pune and UGC New Delhi (F. No. 32-198/2006(SR)) for partial funding. We thank Dr. P.R. Rajamohanan, National Chemical Laboratory for providing NMR data and useful suggestions. The time correlated single photon-counting spectrophotometer facility in the Department was created by funding from the University Grants Commission, New Delhi, under the Centre for Advanced Studies funds (CAS). We thank Dr. A.V. Sapre for helpful discussion on fluorescence measurements. We thank SAIF, Lucknow for providing ESI-MS data.

Supporting Information Available: Luminescence decay lifetime of the complexes **1**−**4** in the presence of CT-DNA (Table S1), ^{1}H NMR and H−H COSY spectra of bxbg and complexes **1**−**4** (Figure S1−S5), ESI-MS spectra's of bxbg ligand and complexes **1**−**4** (Figure S6), absorption spectra of complexes **1**−**4** (Figure S7), cyclic voltammograms of complexes **2**−**4** (Figure S8), spectroelectrochemistry of complexes **2**−**4** (Figure S9−S11), H−H COSY and ^{1}H NMR dilution spectra's of complex **2** in D_2O (Figure S12), NOESY spectra's of complex **2** at different concentrations (Figure S13), SEM images complex **2** (figure S14), X-ray powder diffractogram of complexes **1**−**4** (Figure S15), emission spectra of Ru(II) complexes **1**−**4** in phosphate buffer with increasing [DNA]/[Ru] ratio from 0 to 30 (Figure S16), emission spectra of Ru(II) complexes **1**−**4** using anionic quencher $K_4[Fe(CN)_6]$ in the presence and absence of DNA in phosphate buffer (Figure S17). This material is available free of charge via the Internet at http://pubs.acs.org. CCDC 736729 contains the supplementary crystallographic data for **2**. The data can be obtained free of charge via www.ccdc.cam.ac.uk/conts/retrieving.html (or from the Cambridge Crystallographic Data Centre, 12 Union Road, Cambridge CB2 1EZ, U.K.; fax: (+44)1223−336−033; or deposit@ccdc.cam.uk).